Petroleum Science (2018) 15:211–229
https://doi.org/10.1007/s12182-018-0232-3

ORIGINAL PAPER

Cover article

Diagenetic and geochemical studies of the Buchan Formation (Upper Devonian) in the Central North Sea

Long-Xun Tang[1] · Jon Gluyas[1] · Stuart Jones[1] · Leon Bowen[2]

Received: 24 October 2017 / Published online: 3 May 2018

Abstract
The Upper Devonian Buchan Formation reservoirs in the UK Central North Sea are litharenite/sublitharenite and were deposited in fluvial–aeolian settings. The grain-coating clays in the aeolian sandstones have effectively inhibited quartz overgrowth. Hence, the reduction of reservoir quality is mainly due to mechanical compaction and early dolomite precipitation in both fluvial and aeolian sandstones; quartz overgrowth and kaolinite illitization in fluvial sandstones; and limited smectite illitization in aeolian sandstones. The carbon/oxygen stable isotopes of dolomite cements suggest a predominantly marine carbon source and precipitation temperatures between 25 and 58 °C indicating a shallow burial depth during dolomite precipitation. The temperatures and the dolomite distribution indicate that the cements originated from the overlying Upper Permian Zechstein carbonates. Extensive quartz overgrowths formed at 80 and 120 °C in the late and deep diagenetic burial history. The most probable silica source was from feldspar kaolinitization and pressure dissolution of quartz grains. Through detailed petrography and geochemical analyses, the burial–paragenesis–thermal history of the Buchan Formation has been constructed. Similar diagenetic processes are likely to have occurred in the Buchan Formation in other parts of the Central and Northern North Sea. This study may allow new petroleum plays to be considered in areas previously thought to have poor hydrocarbon potential.

Keywords Buchan Formation · Upper Devonian · Central North Sea · Sandstone diagenesis · Geochemistry methods

1 Introduction

The Upper Devonian Buchan Formation has a wide distribution in the Central and Northern North Sea (Ziegler 1990) but is usually perceived to have little hydrocarbon potential (Downie 2009). Despite this, a number of discoveries in both the UK and Norwegian North Sea have confirmed considerable, but highly variable hydrocarbon reserves in the Buchan Formation (Edwards 1991; Trewin and Bramwell 1991; Knight et al. 1993; Gambaro and Currie 2003; Gluyas et al. 2005). Until now, the Buchan Formation has been poorly understood due to the fact that the Devonian strata were never considered as the main exploration targets for petroleum. Previous studies of the Upper Devonian reservoirs have concentrated on the sedimentology, describing the strata as deposits of fluvial-braided and aeolian systems (Marshall and Hewett 2003; Downie 2009).

The reservoir quality of these typically terrestrial deposits is highly heterogeneous and varies from nearly impermeable (less than 0.1 mD) up to Darcy level (Gluyas et al. 2005). It is reported that cementation by authigenic carbonate and quartz overgrowth are the principal causes of poor reservoir quality (Downie 2009). However, no detailed report has explained the sources of these cements, when and under what conditions they were formed and how the cements control the reservoir quality.

To achieve a better understanding on these problems, the Ardmore Field (previous name 'Argyll') was selected as the main research target due to there being extensive core coverage of the Buchan Formation interval. The

Edited by Jie Hao

✉ Long-Xun Tang
longxun.tang@outlook.com

[1] Department of Earth Sciences, Durham University, South Road, Durham DH1 3LE, UK

[2] Department of Physics, Durham University, South Road, Durham DH1 3LE, UK

Ardmore Field has multiple reservoirs in Permian Zechstein carbonate, Permian Rotliegend sandstone and Upper Devonian Buchan Formation all of which are in communication, together with minor, isolated oil accumulations in the Upper Jurassic Fulmar Sandstones and Upper Cretaceous Chalk (Bifani and Smith 1985; Robson 1991; Gluyas et al. 2005). The properties of the two Permian units have been recognized in numerous studies (e.g. Nagtegal 1979; Glennie and Provan 1990; Purvis 1992; Howell and Mountney 1997; Leveille et al. 1997; Sweet 1999; Heward et al. 2003; Gluyas 2016); but this is the first time a study has been reported on the combined diagenetic and geochemical analyses of the Buchan Formation. The results provide new insights into these poorly understood Devonian reservoirs. We investigate the sources of cements, diagenetic history and evaluate their influences on reservoir quality. Additionally, the outcomes have implications for the future petroleum explorations of Devonian age reservoirs in the Central and Northern North Sea.

2 Geological setting

The Ardmore Field is located on the Argyll Ridge, a large NE–SW trending Palaeozoic-age tilted fault block on the south-western flank of the Central Graben in Block 30/24, UK Continental Shelf, about 300 km east from Edinburgh. The field measures 2.5 km wide and 6 km long (Fig. 1a). It is a horst feature with the crest in the north and fault closure to the north-east. A combination of dip and faults defines the limits of the field on the north-west and south-east flanks, while dip closure defines the southern limits of the field. The major fault trends are in two main directions, WNW–ESE cut by NW–SE faults. As the Devonian is steeply dipping within the Ardmore Field, it is further dissected by those NW–SE-oriented faults, which divide the field into three parts: the NE, central and SW segments (Fig. 1b).

The Middle Devonian Kyle Limestone and overlying Upper Devonian Buchan Formation are the oldest strata penetrated in the Ardmore Field. The Kyle Limestone shows strong seismic reflection which provides a good lower limit, and its upper boundary is a conformable transition to the Buchan Formation (Fig. 1c). The uppermost Buchan Formation sub-crops at the Base Permian unconformity, the oldest stratigraphic units sub-crop in the NE segment with progressively younger stratigraphic units sub-cropping towards the SW segment. Eleven units (named as B01–B11 from base to top) have been divided within the formation based on well logs utilizing laterally correlative shale beds (Gluyas et al. 2005). The interpretation is controlled by available core data, although this provides limited stratigraphic control, as core coverage per unit is sparse. The lowest units (B01–B03) are of poor reservoir quality, as they are shaley relative to the overlying reservoirs. These older units are oil-bearing in the NE segment of the field, but few wells have penetrated them and only minor oil production has occurred. The reservoir quality of Buchan Formation improves towards the south-west, with the central and south-west segments containing better reservoir quality intervals.

We are uncertain about the depositional facies for sandstones in stratigraphic units B01, B02, B03, B05 and B06 due to the poor core coverage; while the units B04, B09, B10 and B11 are dominated by fluvial-braided deposits, and units B07, B08 and some minor portions in B09 and B10 contain significant aeolian deposits (Fig. 2) (Tang et al. 2017). The overall known units comprise a fluvial (B04)-aeolian (B07 and B08)-fluvial (B09, B10 and B11) variation and generally represent a progradation-retreat-progradation cycle of the alluvial fan-based braided system with aeolian deposits occurring mainly between two main progradation periods (Tang et al. 2017). The total thickness of Buchan Formation is nowhere fully penetrated, but based on seismic interpretation we estimate it to be up to 800 m.

The Buchan Formation in the Ardmore Field is heterogeneous, and hence, the reservoir quality is highly variable. The net-to-gross ratio is commonly greater than 70% in the better quality zones, the better developed braided channels and aeolian dune sand bodies achieve porosity between 12% and 28%, and the typical porosity values of North Sea oil-bearing sandstones at this depth is around 16% (Selley 1978). Net sand permeability reaches 5 Darcies, though 10 s of mD and 100 s of mD are typically average values in the fluvial and aeolian sand packages, respectively.

3 Database and methods

One hundred and one Buchan Formation core samples were collected from five wells (14 from well 30/24-05, 16 from well 30/24-20z, 38 from well 30/24-28, 16 from well 30/24-31 and 17 from well 30/24-34). Care was taken to minimize breakage and thereby preserve cements, textures and fabrics. Thin sections for petrographic examination, fluid inclusion wafers and other analytical analysis were prepared. Samples for thin section petrography were impregnated with blue epoxy to facilitate the identification of porosity. Petrographic examination was performed on a Leica DM2500P standard polarizing microscope to identify textures and mineral composition as well as to characterize the relationships between different cement types. Photomicrographs were taken using an attached Leica DFC420C digital camera. Estimation of the percentages of detrital grains and cements was made on thin sections by

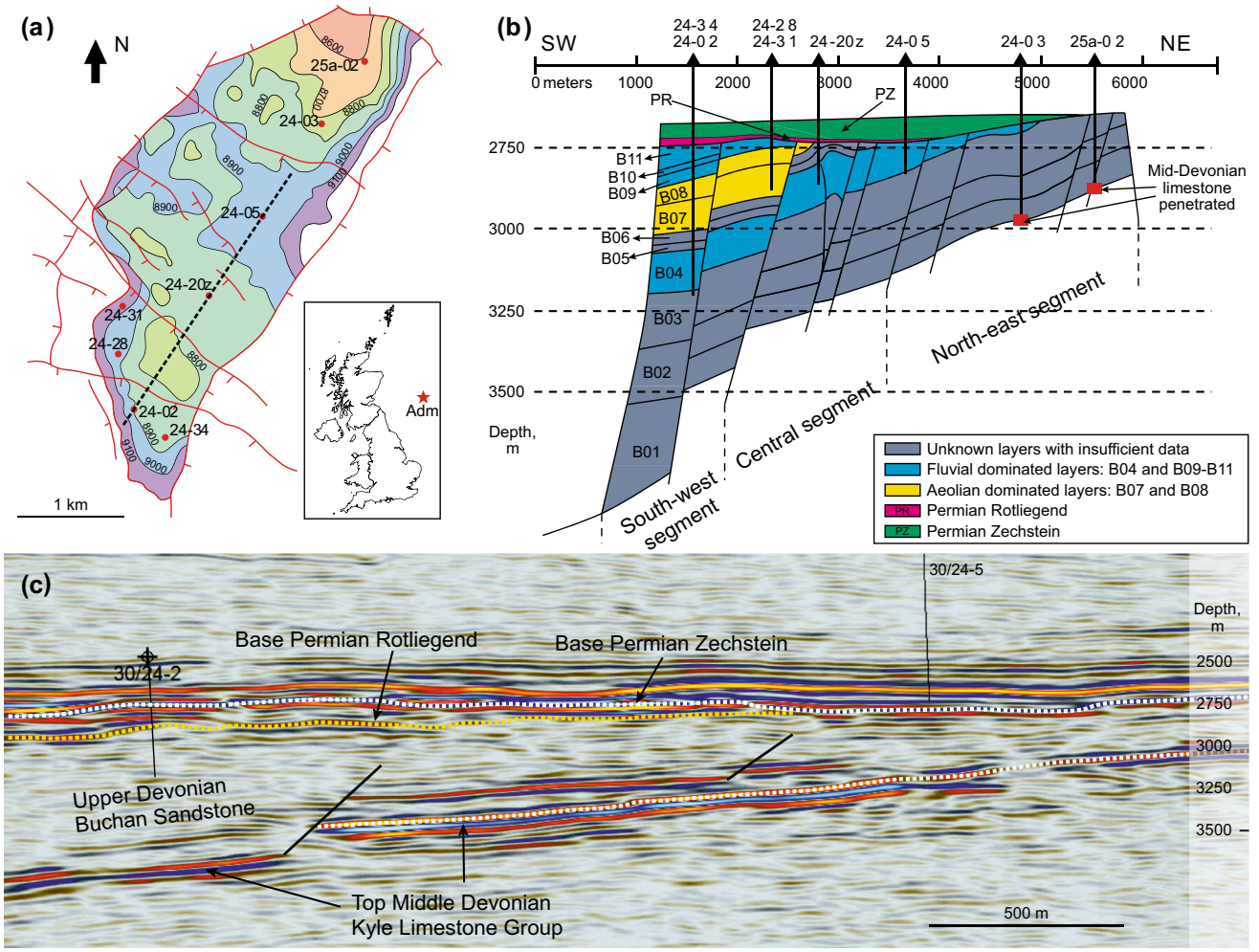

Fig. 1 Geological maps showing: **a** location and main structure elements of the Ardmore (Adm) Field. **b** Vertical section of SW–NE profile. **c** Seismic section of SW–NE profile (dash line in Fig. 1a)

point counting analysis (n = 300). The measured porosity and permeability data were provided by EnQuest internal reports.

Based on the microscopic petrography examinations, representative samples were selected for Hitachi SU70 scanning electron microscope (SEM) observation. The electron beam used had an acceleration energy of 10–20 kV. Backscattered scanning electron microscope (BSEM) is also applied, and the technique relies on backscattered electrons on polished sections to define mineral grain boundaries, and then analyses of X-ray emission with an energy-dispersive X-ray detector (EDX) to assign the mineral compositions. Cathodoluminescence (CL) was employed for recognizing different quartz overgrowth generations using a Gatan Mono CL Digiscan II, operated at 12 kV for panchromatic imaging.

To identify and quantify the clay mineralogy, six samples were chosen for XRD analysis (4 from grain-coated aeolian sandstone samples and 2 from fluvial sandstone samples with quartz and dolomite cements and without grain coatings). The bulk rock was disaggregated by gentle crushing and suspended in distilled water. After allowing the coarse grains to settle for 3 h, the clay in suspension was decanted into a tube for centrifuging. Clay less than 2 microns was tested after being air-dried, treated with glycerol and heated at 500 °C for 2 h.

A very fine-grained sample (siltstone) was selected for quantitative evaluation of minerals by scanning electron microscopy (QEMSCAN) analysis with the aim of providing a quantitative petrographic characterization. The sample was cut to give a flat surface and impregnated with Struers Epofix resin within a 30-mm-diameter mould. The samples were polished, carbon-coated and measured at the Rocktype QEMSCAN facility. The FEI QEMSCAN technique combines SEM and X-ray (EDX) technology to provide automated petrographic descriptions of geological samples in the form of high-resolution images and spatially resolved compositional and textural data.

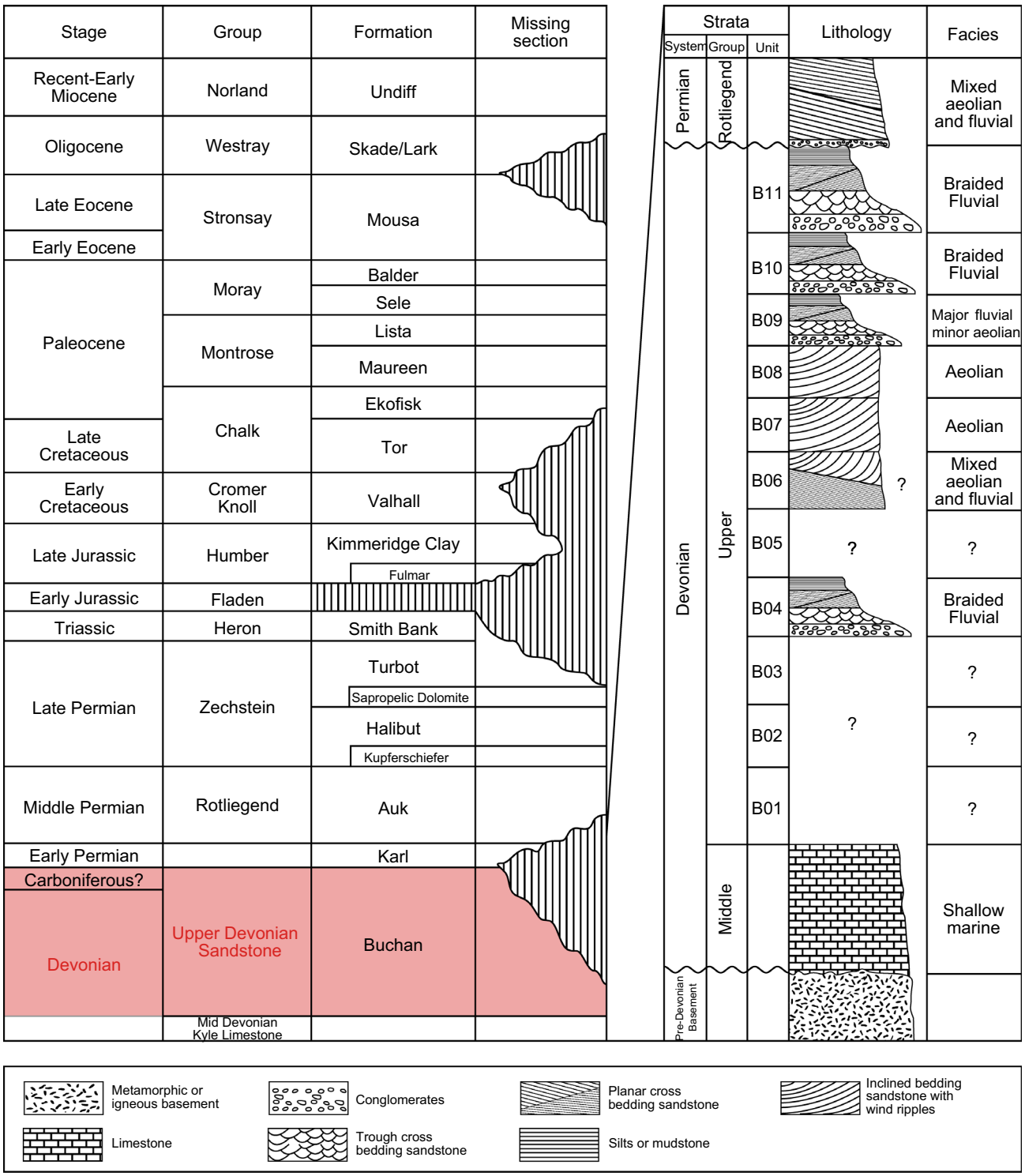

Fig. 2 Stratigraphy and sketched sedimentary log of the Ardmore Field

Doubly polished wafers for fluid inclusion analysis were prepared from 11 samples selected from sandstones with extensive quartz overgrowth; the aim is to investigate the precipitation temperature of the quartz overgrowth. Homogenization temperatures (T_h) of fluid inclusions were measured by the Linkam THMS600 Cooling-Heating Stage in State Key Laboratory of Oil and Gas Reservoir Geology and Exploitation, Chengdu University of Technology (CDUT). The temperature range of the instrument is from −196 to 600 °C with a precision of < 0.1 °C. The rate of

temperature increase can be controlled to within 1 °C/min when approaching the critical point.

The carbon and oxygen isotopic analysis on carbonate cements was measured by the Scottish Universities Environmental Research Centre (SUERC) in the University of Glasgow. Seventeen sandstone samples with variable amounts of dolomite cements were gently disaggregated with a hammer and then crushed in a mortar; at least 1 mg of dolomite powder is obtained for each sample. The value of $\delta^{13}C$ and $\delta^{18}O$ was determined on CO_2 liberating from dolomite cements dissolved by 100% H_3PO_4 at 50 °C. The isotopic composition of CO_2 is reported in units of ‰ relative to Pee Dee Belemnite (PDB).

Burial history and thermal conditions of the Ardmore Field have been analysed using data from exploration wells by the Schlumberger software PetroMod (V2014.1). In the studied area, there are several stratigraphic hiatuses between the Devonian and Palaeogene, with the estimated thicknesses calculated by using data from adjacent fields (Marshall and Hewett 2003; Hayward et al. 2003; Glennie 2009). The maximum burial depth of the Upper Devonian Buchan Formation in the Ardmore Field occurs today at approximately 2.7–3.2 km. The present-day geothermal gradient is around 34.6 °C/km (Marshall and Hewett 2003) with an average surface temperature of 12 °C, and the present-day maximum temperature is around 115–120 °C at 3.2 km burial depth.

4 Results

4.1 Petrography

Petrographic examination indicates that the fluvial and aeolian sandstones have a different mineral composition and grain texture. Generally, the sandstone samples are classified as litharenite to sublitharenite according to Folk (1980), with a total average composition of $Q_{78}F_3R_{19}$, and the aeolian sandstones have a more mature composition ($Q_{82}F_2R_{16}$; Fig. 3b) than fluvial sandstones ($Q_{76}F_3R_{21}$; Fig. 3a). Texturally, except the minor thin-bedded (less than 1 m) and sandy-clast-supported conglomerates (less than 10% among all fluvial deposits) and mudstones (less than 10% among all fluvial deposits), the fluvial sandstones are relatively immature and fine- to medium-grained. Sorting ranges from poor to moderate, and roundness of grains varies from sub-angular to sub-rounded. Quartz grains are tightly compacted usually showing curved and rare concavo-convex grain contacts. The fine- to medium-grained aeolian sandstones have a higher textural maturity, sorting ranges from moderate to good, and roundness of grains varies from sub-rounded to rounded. The grain contacts are commonly point to long.

Detrital quartz is the dominant mineral type (41%–95%) in all samples; most quartz grains are monocrystalline with 0.15–0.3 mm grain size (Fig. 4a) and can exhibit undulose extinction (Fig. 4b). Detrital feldspar occurs from trace amounts up to 7% with the main feldspars commonly demonstrating polysynthetic twinning microcline (Fig. 4c). The feldspars occur as both fresh grains and dissolved grains with relic outlines (Fig. 4c, d). Other major identified minerals include mica comprising up to 13% and showing variable amounts of distortion and grain breaking (Fig. 4e). Rock fragments are in variable quantities and include micaceous and illitic mud clasts and fine-grained metamorphic and volcanic fragments to a lesser quantity (Fig. 4f).

Diagenetic minerals in the Buchan Formation include dolomite, quartz overgrowth, kaolinite, illite and illite/smectite (I/S). Dolomite occurs in both fluvial and aeolian sandstones (up to 28%, mean value 7.5%) showing sporadically 'spotty' purple-red-stained cements and sometimes in irregular band distribution in hand specimen (Fig. 5a). Under thin section observation, the poikilotopic dolomite cements commonly show typical structures of 'light rims and cloudy core' in a well-developed rhombic shape and size ranges from 20 to 200 μm (Fig. 5b). Chlorite occurs in both fluvial and aeolian sandstones with a trace amount (up to 0.5%), confirmed by XRD analysis (see Table 1).

Apart from the prevalent dolomite cements, fluvial sandstones contain dense authigenic kaolinite aggregates and extensive quartz overgrowths. The authigenic kaolinite is present as densely packed pseudo-hexagonal booklets and platelets as grain-shaped masses and pore-filling aggregates in the interstices (Fig. 5c). The quartz overgrowths (1%–7%, mean value 4.5%) occur as syntaxial cements forming incomplete or complete rims around quartz grains with the thickness ranging from 10 to 50 μm. Boundaries between detrital quartz grains and overgrowth are visible due to the presence of 'dust' lines (Fig. 4a). The SEM-cathodoluminescence (CL) analysis revealed that the quartz overgrowths were probably formed in several stages (Fig. 5d, e), which correspond to the range of measured homogenization temperature in the fluid inclusion (80–120 °C). Authigenic illite can be seen in SEM images and mainly occurs as fibrous or hairy crystals (Fig. 5f).

Conversely, quartz overgrowth is absent and kaolinite is subordinate in aeolian sandstones. Illite/smectite (I/S) has been identified by EDX spectrum (Fig. 5h) and XRD analysis (Table 1) which is the unique and most important clay type in aeolian sandstones although it is present in minor amounts (0.5%–5%). Thin section and SEM observations illustrate that the I/S occurs in two forms. (1) The grain-coating I/S (Fig. 5g) commonly occurs as cornflake and/or honeycomb morphology with short filamentous

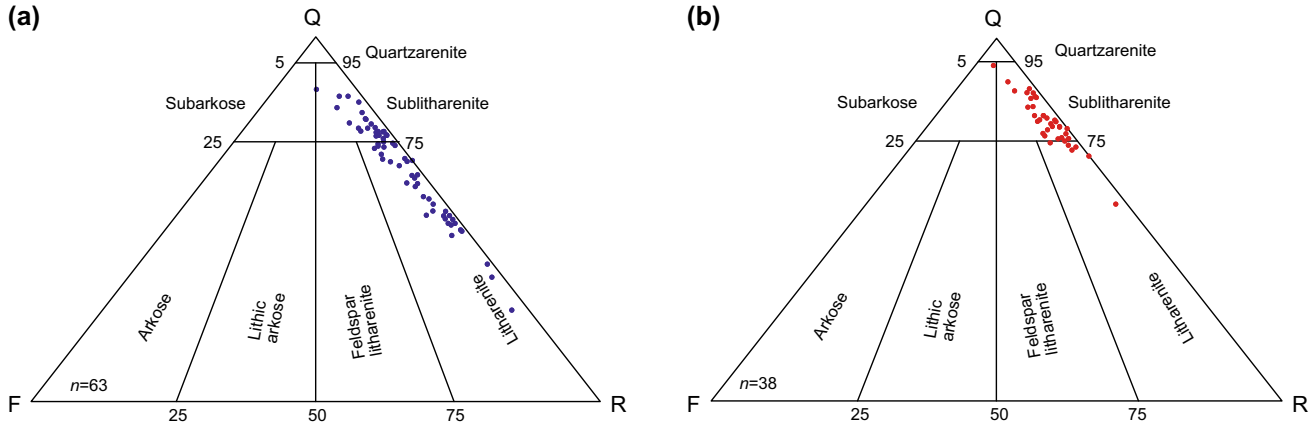

Fig. 3 The QFR ternary charts for **a** fluvial sandstone samples; **b** aeolian sandstone samples

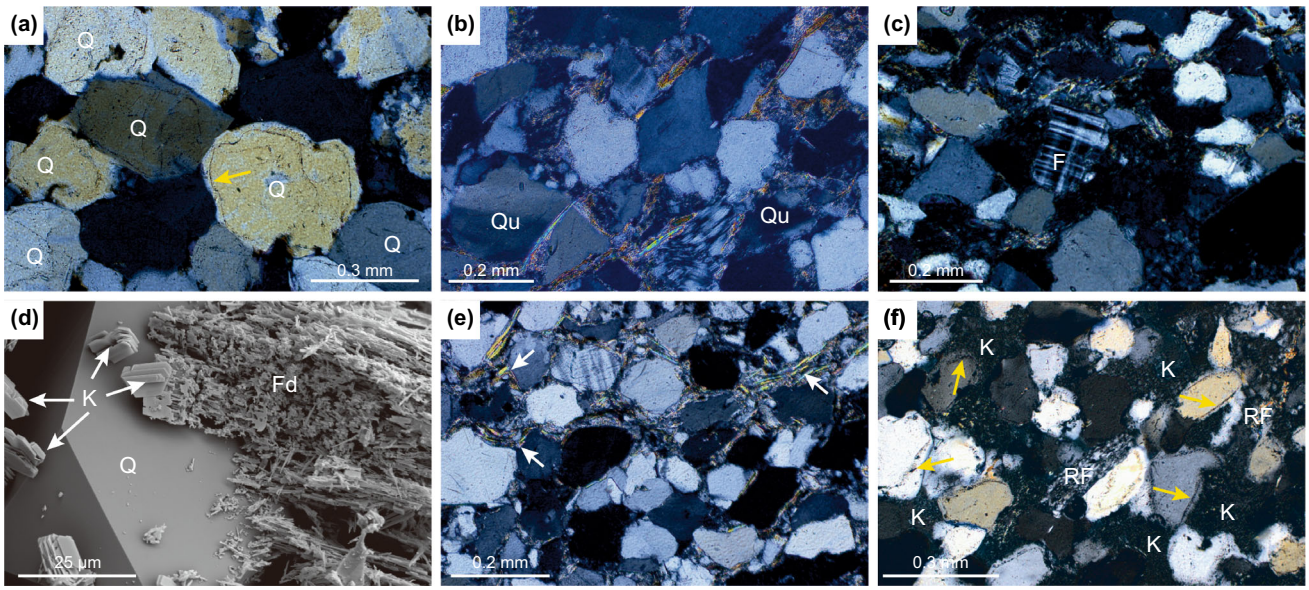

Fig. 4 Photomicrographs of sandstone compositions. **a** Monocrystalline quartz grain with quartz overgrowth and visible dust rims (yellow arrows) on the original detrital grain. Well 30/24-34, 2967.8 m. **b** Quartz grains exhibiting undulose extinction. Well 30/24-20z, 3125.4 m. **c** Microcline showing polysynthetic twinning. Well 30/24-05, 2846.4 m. **d** SEM image of feldspar dissolution and presence of authigenic kaolinite. Well 30/24-20z, 3126 m. **e** Bended mica (white arrows) between quartz grains. Well 30/24-20z, 3125.4 m. **f** Possible volcanic-origin rock fragments. Note the pore-filled kaolinite aggregates and quartz overgrowth (yellow arrows). Well 30/24-05, 2847 m. Q, quartz; Qu, quartz with undulose extinction; F, feldspar; K, kaolinite; Fd, dissolved feldspar; RF, rock fragments; D, dolomite; P, porosity

terminations and consists of 1- to 5-μm-thick rims coating all detrital grains in the aeolian sandstones; these grain coatings are absent in fluvial sandstones. Quartz overgrowths are noticeably absent in the aeolian sandstone facies where uniform and robust grain-coating I/S has developed. (2) Pore-filling I/S can occur (< 5%) as aggregates existing in the intergranular pore space of aeolian sandstones and is absent from the fluvial sandstones (Fig. 5i).

4.2 Fluid inclusions

Fluid inclusion thermometry can provide useful temperature information for the authigenic mineral precipitation (Robinson and Gluyas 1992). The fluid inclusions in the selected samples primarily occur in two forms: (1) the belt-like distribution along the healed micro-fractures within quartz grains (Type I; Fig. 6a) and (2) between the host quartz grain and their surrounding overgrowth (Type II; Fig. 6b). The size of fluid inclusions is about 2–8 μm in diameter, and most of them have gas bubbles and fluid

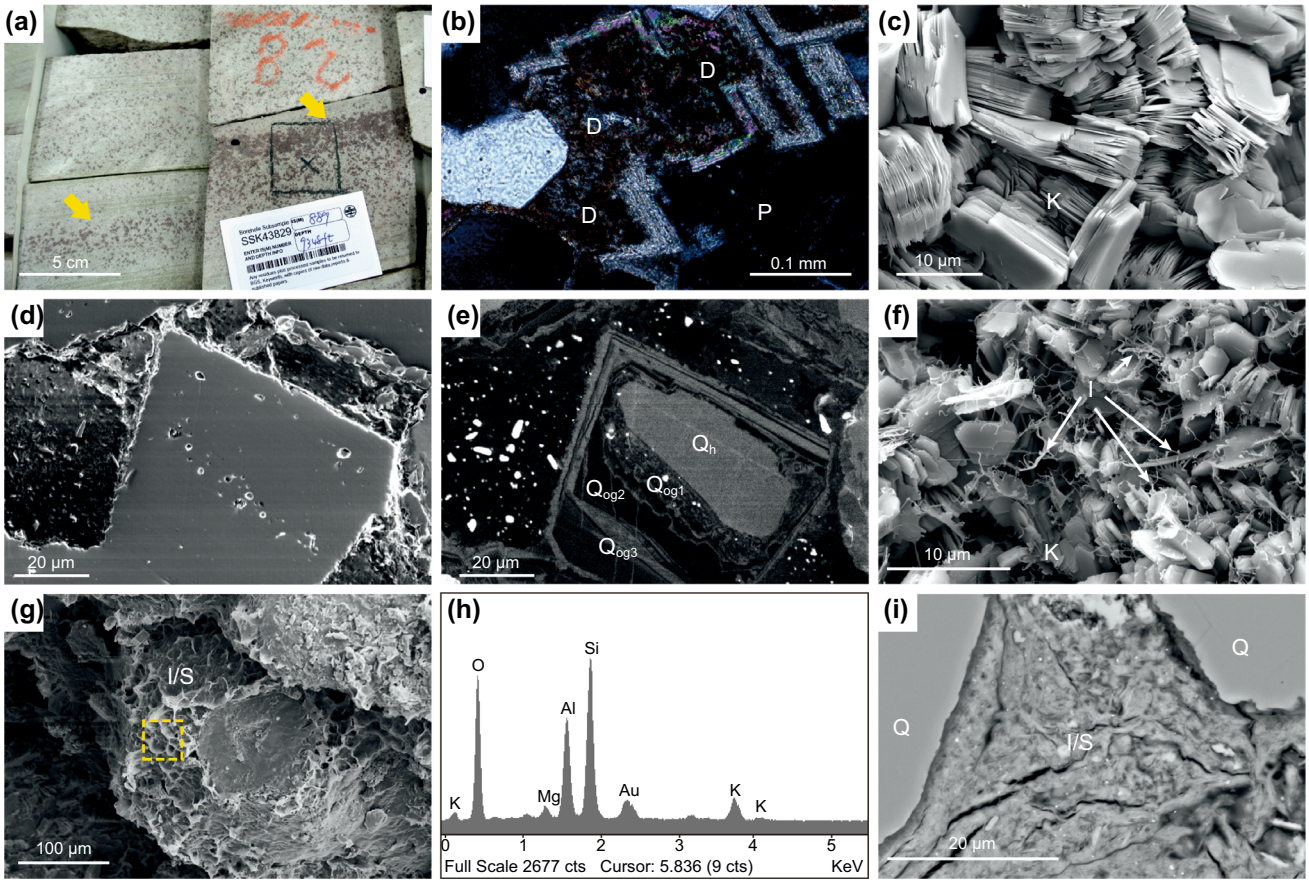

Fig. 5 **a** Thin bands of 'spotty' red-brown-stained cements (yellow arrows) in the cores. Well 30/24-05, 2849.1 m. **b** Dolomite cements in the pore space showing well the rhombic shapes with cloudy cores and light rims under the microscope. Well 30/24-05, 2849.1 m. **c** SEM image of authigenic kaolinite presents in densely packed pseudo-hexagonal booklets and platelets. Well 30/24-05, 2849.1 m. **d** Quartz grain with intense quartz overgrowth under SEM. Well 30/24-34, 2976.4 m. **e** CL image of quartz grain in Fig. 5d. Note the multiple stages of overgrowth around the host grain. Well 30/24-34, 2976.4 m. **f** SEM image of authigenic illite occurring as fibrous and hairy crystals associated with kaolinite aggregates. Well 30/24-05, 2850.9 m. **g** SEM image of grain-coating illite/smectite showing cornflake–honeycomb morphology. Well 30/24-31, 3190.6 m. **h** The EDX spectrum of grain coating I/S (the dashed square area in Fig. 5g). Well 30/24-31, 3190.6 m. **i** BSEM image of pore-filling illite/smectite occurred as flocculent aggregates existing in the intergranular pore space. Well 30/24-31, 3190.6 m. Qh, host quartz grains; Qog, quartz overgrowth; K, kaolinite; I, illite; I/S, illite/smectite; gc, grain coating; pf, pore-filling

phases with a gas–liquid ratio less than 5% at room temperature (15 °C).

The measured homogenization temperature (T_h) of the two-type fluid inclusions is given in Table 2, and Fig. 6 presents the T_h distribution of fluid inclusions in both Type I and Type II. The T_h in the healed micro-fractures mainly ranges from 110 to 140 °C, and a few of them are under 110 °C or over 140 °C. For the Type II fluid inclusions, T_h has a relatively uniform range from 80 to 120 °C with a mean value of 101.2 °C; more than half (56.3%) measured T_h values are located between 81 and 100 °C, which might imply the temperature condition for precipitation of the primary quartz overgrowth.

4.3 Isotopic composition of dolomite cements

The carbon and oxygen isotopic compositions of dolomite cements were measured in 17 sandstone samples (Table 3). The results show that most dolomite cements have a relatively wide range of $\delta^{18}O_{PDB}$ values from − 6‰ to 0.8‰ but are mainly allocated between − 3‰ and 0‰ with an average value of − 1.8‰; $\delta^{13}C_{PDB}$ values vary from − 3.1‰ to 1.6‰. The calculated value of $\delta^{18}O_{SMOW}$ is derived from: $\delta^{18}O_{SMOW} = 1.03091 \times \delta^{18}O_{PDB} + 30.91$ (Coplen et al. 1983), and the temperature is calculated by using fractionation equation between carbonate and water: $1000 \times \ln\alpha_{dolomite-water} = 3.06 \times 10^6/T^2 - 3.24$ (Matthews and Katz 1977).

Table 1 XRD data for < 2-μm-size mineral fraction in selected samples

Well	Depth, m	wt%	Illite/smectite				Illite			Kaolinite			Chlorite			Quartz		Calcite		Dolomite	
		< 2μm	%A	%B	Order	%Illite	%A	%B	Crys	%A	%B	Crys	%A	%B	Crys	%A	%B	%A	%B	%A	%B
30/24-28	2790.14	1.9	34.4	0.7	O	70–80	58.3	1.1	P	0.0	0.0	–	7.1	0.1	P	0.3	0.1	0.0	0.0	0.0	0.0
30/24-28	2829.76	3.0	46.3	1.4	O	70–80	25.9	0.8	P	22.6	0.7	M	2.9	0.1	M	2.4	0.1	0.0	0.0	0.0	0.0
30/24-28	2844.09	3.0	50.5	1.5	O	70–80	32.7	1.0	P	7.5	0.2	M	3.5	0.1	M	5.8	0.2	0.0	0.0	0.0	0.0
30/24-31	3190.34	2.0	44.8	0.9	O	70–80	34.9	0.7	P	10.7	0.2	M	5.1	0.1	P	4.5	0.1	0.0	0.0	0.0	0.0
30/24-18	2794.71	3.3	TR	TR	–	–	22.0	0.7	P	58.7	1.9	M	15.8	0.5	M	3.6	0.1	0.0	0.0	0.0	0.0
30/24-05	2849.27	3.2	TR	TR	–	–	8.5	0.3	P	72.6	2.3	M	5.3	0.2	P	3.1	0.1	0.0	0.0	10.6	0.3

A = weight% relevant size fraction; B = weight% bulk sample

Mixed-layer ordering: RI = randomly interstratified (R0); O = ordered interstratification (R1); LR = long-range ordering (R3)

Crystallinity: VW = very well crystallized; W = well crystallized; M = moderately crystallized; P = poorly crystallized

5 Discussion

5.1 Sources of the authigenic minerals

5.1.1 Authigenic kaolinite and quartz overgrowth

Precipitation of authigenic kaolinite and formation of quartz overgrowth occurred relatively late in the diagenetic history. For the deeply buried sandstones, the concentration of SiO_2 (aq) (< 100 ppm) and Al^{3+} (< 10 ppm) is commonly low (Bjorlykke and Jahren 2012; Yuan et al. 2015); in such a condition with considerable heterogeneity in porosity and permeability, none of the advective flow, thermal convection and diffusion is capable of long-distance and massive transfer of SiO_2 (aq) and Al^{3+} from the remote external sources (Bjørlykke et al. 1988; Yuan et al. 2015).

For the authigenic kaolinite in sandstones, Shelton (1964) suggested three possible sources: (1) crystallization of introduced material from solutions and/or deposition of material from colloidal suspensions; (2) alteration in place of some parent minerals; and (3) recrystallization of fine-grained detrital kaolinite clay. In this study, the authigenic kaolinite mainly presents in two forms (Fig. 7): (1) relatively isolated patches of pore-filling aggregates and 2) aggregates with a recognizable precursor grain shape. With the observed petrographic features and no obvious clue of an external source, the most likely source for authigenic kaolinite is the dissolution of feldspars within the sandstones. On the thin section scale, an inverse correlation could be identified between quantity of remained feldspar and kaolinite (Fig. 8b), that is little remaining feldspar is commonly accompanied by massive kaolinite, and massive remaining feldspar is commonly accompanied by little kaolinite. The inverse correlation between remaining feldspar and kaolinite suggests that the most likely source of kaolinite is the dissolution of local feldspars and/or the dissolved solution from the nearby sandstones. At the same time, the authigenic kaolinite content increases slightly with increasing burial depth (Fig. 8a); this suggests that the higher temperature and deeper burial depth would probably promote the feldspar dissolution and therefore generate more kaolinite.

In quartz-dominated sandstones with quartz overgrowths, the most probable source of silica is from quartz dissolution along grain contacts (commonly stylolite) and feldspar dissolution (Walderhaug 2000; Tournier et al. 2010). The feldspar alteration, in this case kaolinitization, could release considerable amounts of silica ions (Bjørlykke 1983). In this study, the sandstones experienced minor pressure dissolution; additionally, both the authigenic kaolinite and released silica are the products of

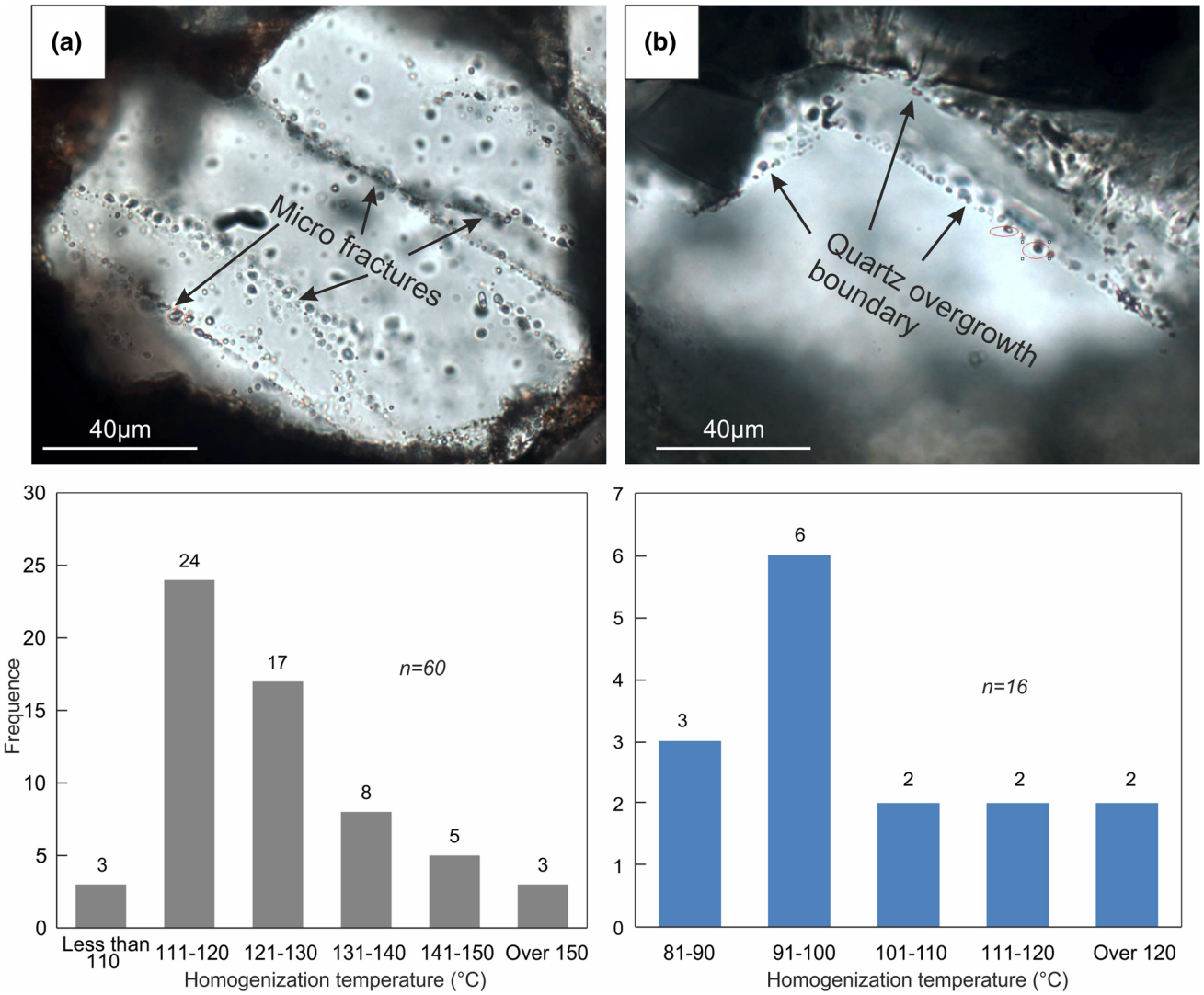

Fig. 6 Photomicrographs and temperature distribution charts of fluid inclusions **a** in the micro-fractures within quartz grains (Type I); **b** between host quartz grains and overgrowth (Type II). Note at least two stages of quartz overgrowths have been observed

feldspar dissolution, and there is indeed a positive correlation between authigenic kaolinite and quartz overgrowth (Fig. 8c). It is proposed in this study that the most probable silica source for quartz overgrowth is the dissolution of local feldspars and pressure dissolution has provided a minor contribution.

5.1.2 Dolomite

Syn-depositional dolomite commonly occurs in sabkha deposits when the Mg–Ca ratio in the brines increased as a result of Ca^{2+} removal from solution (Evans et al. 1969; Kinsman 1969). If this was the case for the dolomite in the Buchan Formation, the distribution of dolomite cements would expect to be highly facies-related, such as with the interdune sabkha and desert lakes. However, the dolomite cements are found throughout the cored intervals, regardless of lithofacies, and occur in both aeolian and fluvial sandstones.

The $\delta^{13}C_{PDB}$ values are largely but slightly negative and restricted near 0‰ (14 out of 17 are between − 3.0‰ and 1‰ mean value − 1.2‰; Table 3) which may indicate a major contribution from a marine carbon source (Keith and Weber 1964) and minor from other sources. Talbot (1990) has suggested that the correlation coefficient between $\delta^{13}C_{PDB}$ and $\delta^{18}O_{PDB}$ is a useful tool to discriminate whether the water setting is open or closed; that is, high ($r > 0.7$) and low ($r < 0.4$) coefficients indicate closed and open settings, respectively. The measured samples have a quite low correlation coefficient between $\delta^{13}C_{PDB}$ and $\delta^{18}O_{PDB}$ ($r = 0.46$) which would imply a generally open setting, where fresh sea water was commonly introduced. Therefore, the $\delta^{18}O_{SMOW}$ value of 0‰ of formation water in the eodiagenetic stage is acceptable. By employing the oxygen

Table 2 Thermometry data of fluid inclusions in Buchan Formation from Ardmore Field

Sample		Type	Distribution	Shape of FI	Gas/liquid ratio, %	Homogenization phase	T_h, °C		Salinity (wt% NaCl)
Well	Depth, m						Type I	Type II	
30/24-05	2840.1	Brine	Belt	Regular	≤ 5	Liquid	117–130	83	6.88
	2844.7	Brine	Belt	Regular	≤ 5	Liquid	110–135	97	12.68
	2846.5	Brine	Belt	Regular	≤ 5	Liquid	109–131	87	11.61
	2846.8	Brine	Belt	Regular	≤ 5	Liquid	109–149	101	10.62
		Brine	Belt	Regular	≤ 5	Liquid		92	11.58
		Brine	Belt	Regular	≤ 5	Liquid		93	4.8
		Brine	Belt	Regular	≤ 5	Liquid		121	2.74
	2848.1	Brine	Belt	Regular	≤ 5	Liquid	109–141	118	8.35
		Brine	Belt	Regular	≤ 5	Liquid		94	2.74
	2849.6	Brine	Belt	Regular	≤ 5	Liquid	114–146	123	4.96
		Brine	Belt	Regular	≤ 5	Liquid		87	11.61
	2850.8	Brine	Belt	Regular	≤ 5	Liquid	118–146	103	3.87
30/24–28	2795.0	Brine	Belt	Regular	≤ 5	Liquid	112–137	91	11.05
30/24–34	2903.8	Brine	Belt	Regular	≤ 5	Liquid	111–117	94	8.19
	2903.8	Brine	Belt	Regular	≤ 5	Liquid		117	2.74
	2933.9	Brine	Belt	Regular	≤ 5	Liquid	112–157	118	3.55

T_h Homogenization temperature

Table 3 Stable isotopic data and calculated formation temperature of dolomite cements in the Buchan Formation sandstone samples

Well	Depth, m	Carbonate cement type	Carbonate cement, %	$\delta^{18}O_{PDB}$, ‰	$\delta^{13}C_{PDB}$, ‰	$\delta^{18}O_{SMOW}$ (calculated, ‰)	Temp, °C $\delta^{18}O_{SMOW}$ = 0‰
30/24-03	2692.0	Dolomite	20	0.5	0.0	31.4	24.0
30/24-03	2692.3	Dolomite	5	0.6	1.0	31.5	23.5
30/24-03	2697.8	Dolomite	10	− 0.1	1.2	30.8	26.6
30/24-05	2844.7	Dolomite	20	− 1.0	− 2.4	29.9	30.8
30/24-05	2846.5	Dolomite	3	− 2.4	− 2.6	28.4	37.7
30/24-05	2848.1	Dolomite	10	− 2.7	− 3.0	28.1	39.2
30/24-05	2849.3	Dolomite	10	− 0.8	− 2.4	30.1	29.9
30/24-05	2850.2	Dolomite	20	− 1.3	− 3.1	29.6	32.2
30/24-05	2850.8	Dolomite	10	− 0.7	− 2.1	30.2	29.4
30/24-18	2797.8	Dolomite	40	− 1.7	− 0.1	29.2	34.2
30/24-18	2798.4	Dolomite	15	− 0.5	− 0.3	30.4	28.5
30/24-20z	3120.8	Dolomite	7	− 2.1	− 1.5	28.8	35.9
30/24-20z	3129.9	Dolomite	5	− 2.1	− 2.3	28.8	36.1
30/24-20z	3131.2	Dolomite	10	0.8	− 2.1	31.7	22.8
30/24-20z	3174.5	Dolomite	5	− 6.0	− 2.9	24.7	57.6
30/24-28	2795.0	Dolomite	10	− 0.9	1.6	30.0	30.2
30/24-34	2903.8	Dolomite	10	− 1.7	0.6	29.2	34.2

The calculated $\delta^{18}O_{SMOW}$ (‰) is derived from $\delta^{18}O_{PDB}$ (‰) by the equation: $\delta^{18}O_{SMOW} = 1.03091 \times \delta^{18}O_{PDB} + 30.91$ (Coplen et al. 1983); the equations used for fractionation between carbonates and water are: $1000 \times \ln\alpha$ dolomite/ankerite-water $= 3.06 \times 10^6/T^2 - 3.24$ (Matthews and Katz 1977); T is in Kelvin unit

isotope fractionation factor for dolomite/water (Matthews and Katz 1977), the calculated precipitation temperatures for dolomite cements range mainly from 25 to 58 °C (Table 3), which would indicate that these dolomite cements formed at shallow burial depths.

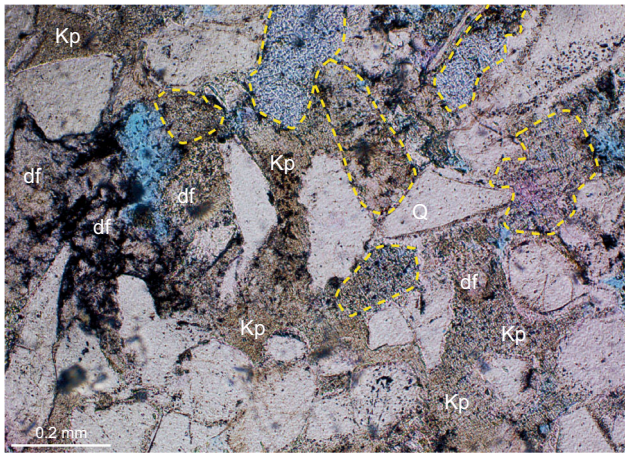

Fig. 7 Different occurrences of authigenic kaolinite aggregates which may indicate at least two different sources. Note the recognizable relic shape of seriously dissolved feldspar grains (yellow dash circles). Well 30/24-34, 2887.7 m. df, dissolved feldspar; Kp, pore-filling kaolinite; Q, quartz

Although there were several major marine incursions in the study area during the Carboniferous, late Permian, late Triassic, Cretaceous, Palaeogene and Quaternary (Bradshaw et al. 1992), this study proposes that the overlying Late Permian Zechstein carbonates would be the most likely source of carbonate cements. A number of comparable cases were reported in the Southern North Sea, therein the dolomite cements (also some other evaporates) are prevalent in the underlying Rotliegend Sandstones, and were precipitated by percolating brines originating directly from the overlying Zechstein carbonates (e.g. Pye and Krinsley 1986; Glennie and Provan 1990; Purvis 1992). It is proposed that this situation would also have occurred in the Ardmore Field. The Upper Devonian Buchan Formation, Permian Rotliegend sandstones and Permian Zechstein carbonates jointly form the reservoir; they were all charged with oil by the stratigraphically younger Jurassic Kimmeridge Clay (Gluyas et al. 2005); this would imply that these three units are in fluid communication. Across the field, the Rotliegend sandstone varies in thickness. It is thicker (around 20 m) in the south-west and centre of the field and thins to the far NE pinching out onto what were pre-Permian (Devonian) topographic highs during deposition (Fig. 9). Thus, Zechstein carbonate directly overlies the Buchan Formation over much of the NE segment of the field. After the Zechstein marine incursion, the Mg^{2+}-rich marine water flowed downwards through the Rotliegend and entered the Buchan Formation, displacing and mixing with the groundwater already present and precipitating dolomite in the interstices. The mixing of the marine water and groundwater probably occurred by a combination of salinity/density differences and diffusion (Purvis 1992). This explanation is strengthened by the distribution pattern of dolomite abundance in these three segments (Fig. 9), and the NE segment has the highest proportion of dolomite cements, while intermediate and minor dolomite cements are shown in the central and SW segments due to part of dolomite having been precipitated in the Rotliegend (Fig. 9). Within the Devonian sequence, there is no clear relationship between abundance of dolomite and the distance between samples and the Devonian/Permian unconformity; this may be attributed to the presence of transmissive faults and fractures. Also, it is unlikely that the post-Permian meteoric water could have entered the Buchan Formation later, owing to the thick Zechstein sediments.

5.1.3 Illite/smectite (I/S)

The cornflake and honeycomb morphology with boxwork structure and curved edges is a good indicator implying that these I/S clays were transformed from smectitic precursors (e.g. Wilson and Pittman 1977; Burley 1984; Keller et al. 1986; Vitali et al. 1999; Wilson et al. 2014). Both the grain-coating and pore-filling I/S, though the average amount is around 5%, are the featured clay types in aeolian sandstones. Several petrographic features can be characterized including: (1) the general occurrence at the grain contact areas; (2) thicker I/S coating in the framework-grain depressions and rough surfaces and (3) thinner I/S coating in the non-depression and smooth areas (Fig. 10). These features closely conform to the criteria set by Wilson and Pittman (1977) for recognizing mechanically infiltrated clays.

In such a mixed fluvial–aeolian setting, especially during the aeolian-dominated period, the fluvial system retreated and only distal sectors of the fluvial distributary system could affect the study area (e.g. sheet flood and floodplain). Additionally, the smectitic clays are usually extremely fine-grained and therefore could be carried further than other sediment grains (McKinley et al. 2003). This observation is supported by the XRD analyses where smectite (shown in illite/smectite) only occurs as trace amounts in the fluvial channel samples (Table 1).

The most likely source of smectite is the fluvial-origin clay-bearing waters which represent the sheet flood and/or floodplain deposits. In the aeolian-dominated period, these sediments could be accumulated in the interdune and/or desert lake environments. The dune sands were dry, porous and permeable shortly after deposition; this clay-bearing water could easily move into grain interstices by downward or lateral migration and form grain-coating and pore-filling clay aggregates before compaction. This interpretation is also reinforced by the QEMSCAN examination undertaken on a sheet flood siltstone sample (Fig. 11), which has

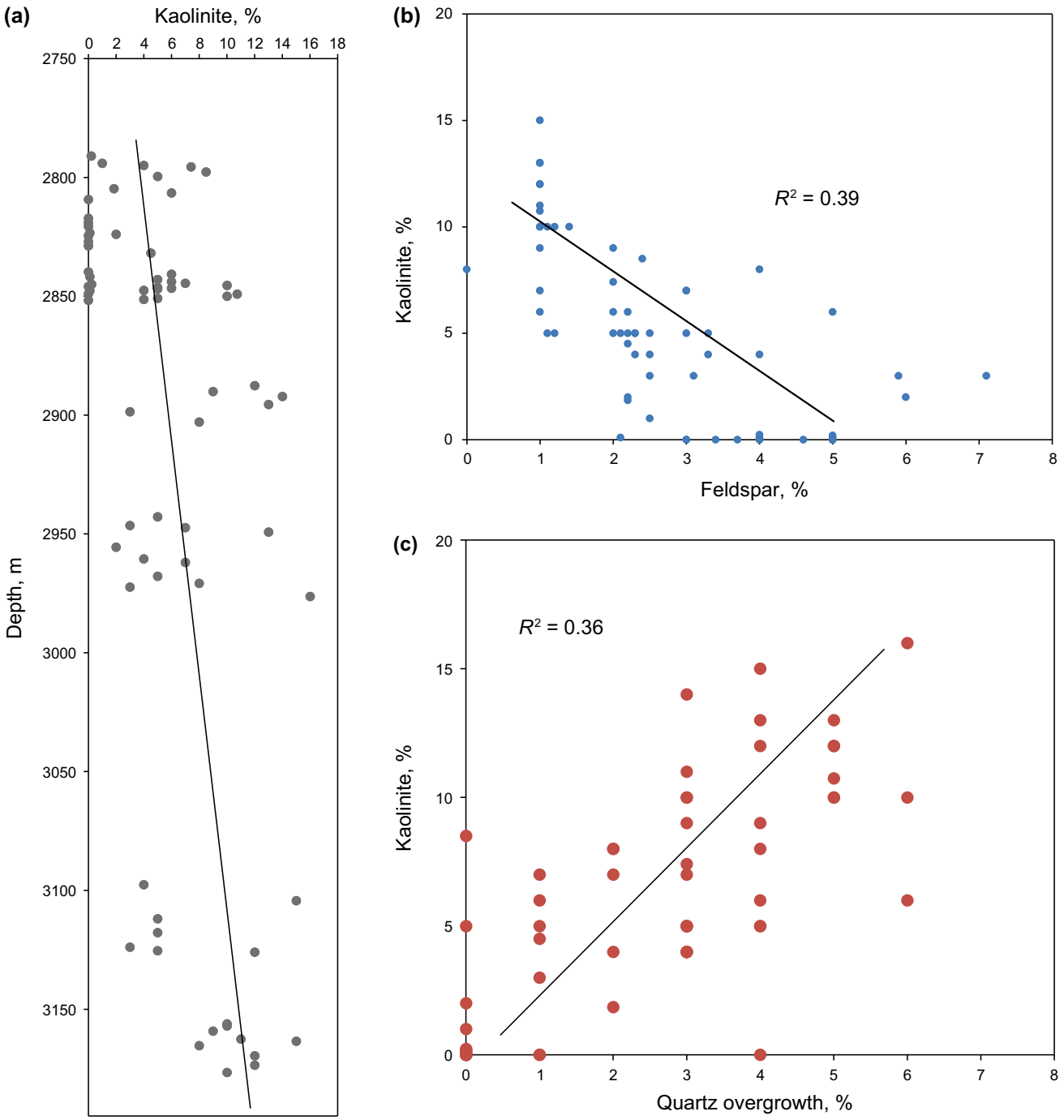

Fig. 8 Scattered diagrams showing relationship between: **a** kaolinite and depth, **b** kaolinite and feldspar, **c** kaolinite and quartz overgrowth. Database is from fluvial sandstone samples

higher illite/smectite content (15.5%) which mainly presents as pore-filling aggregates.

5.2 Paragenesis and burial history

The relative sequence of the major diagenetic events of the Buchan Formation in the Ardmore Field can be determined based on the textural relationships from thin sections and SEM observations. With the constraints set by the clay mineral XRD analysis, calculated temperatures from isotopic composition of dolomite cements, homogenization temperature of fluid inclusions in the quartz overgrowths and the thermal conditions of Ardmore exploration well, a joint paragenesis–burial–thermal history can be generated (Fig. 12).

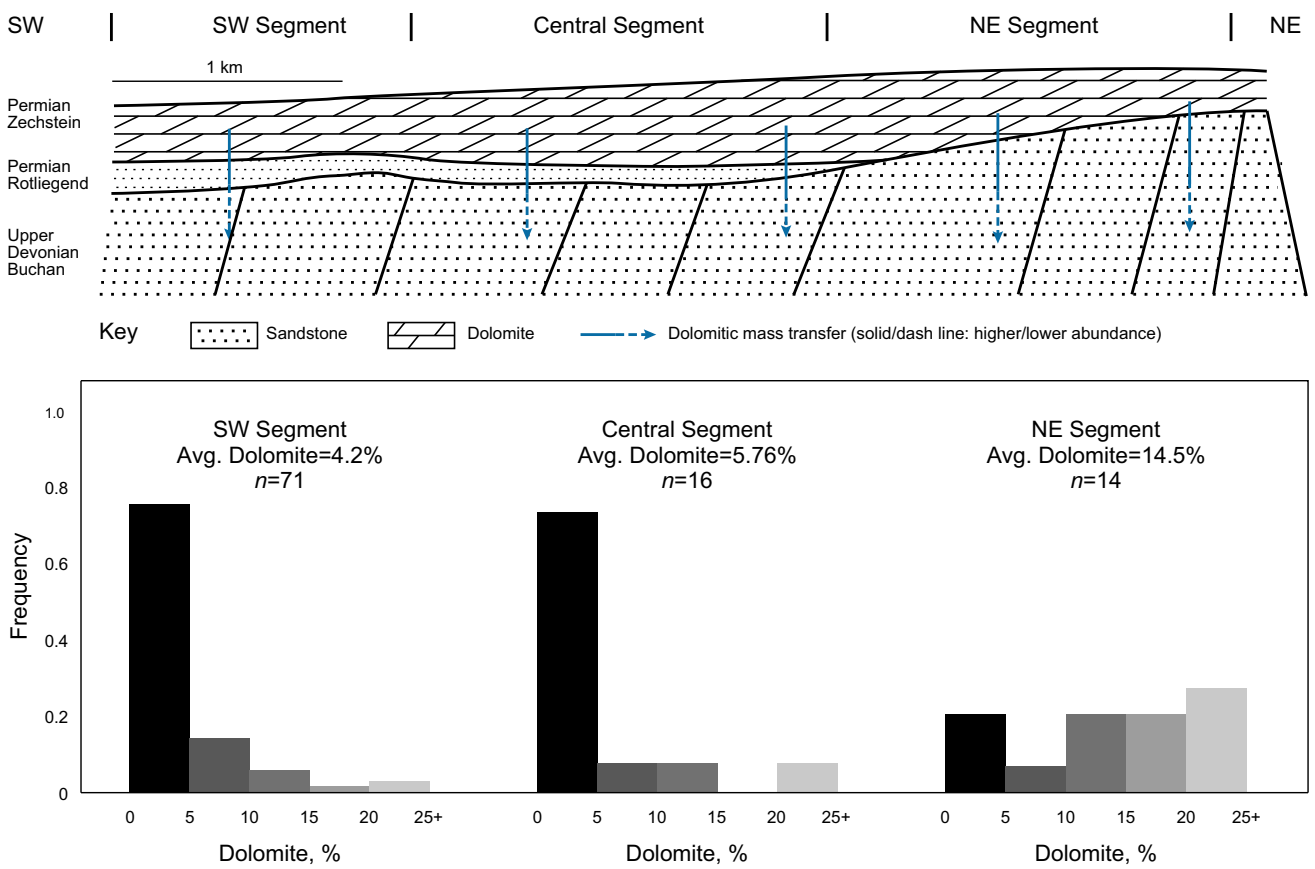

Fig. 9 Sketched map showing dolomite precipitation from Zechstein and the statistics of the dolomite abundance in three segments. Note the vertical thickness is not to scale

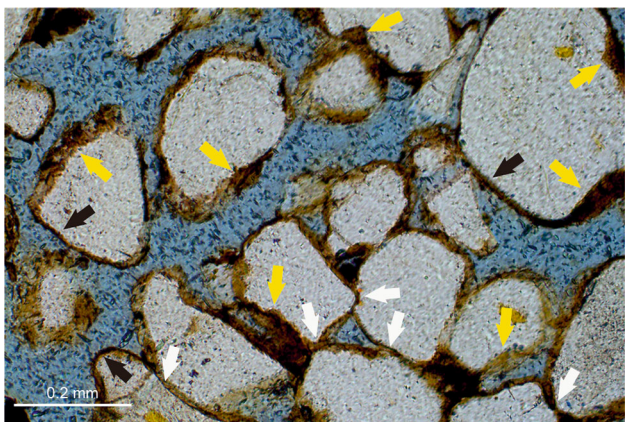

Fig. 10 Photomicrograph showing I/S occurred at the grain contact areas (white arrows), thicker I/S coating in the framework-grain depressions and rough surfaces (yellow arrows) and thinner I/S coating in the non-depression and smooth areas (black arrows). Sample from Well 30/24-31, 3190.6 m

In summary, before mechanical compaction, the earliest event was the infiltration of clay which only occurred in the aeolian sandstones. The dominant eogenetic processes in both fluvial and aeolian sandstones were compaction and dolomite cementation. The burial curves show that the Upper Devonian intervals were consistently at shallow burial depth (< 1 km) until the Palaeogene and then rapidly buried to today's maximum depth around 2.7–3.2 km. The subsequent mesogenetic events mainly occurred since the Palaeogene and include: (1) for the aeolian sandstones, compaction continuously reduced porosity with the increasing depth; illitization might be the final event in the aeolian sandstones, and this is supported by the XRD analysis. There are 70%–80% of illite within I/S which are in ordered interstratification (R1 order), and this usually indicates the temperature is greater than 100 °C (Hoffman and Hower 1979; Huang et al. 1993); and (2) for the fluvial sandstones, it is not easy to determine the accurate sequence of the quartz pressure dissolution and feldspar dissolution/authigenic kaolinite generation. As the most possible source of silica, these processes are certainly prior to the quartz overgrowths which occurred in a formation temperature range of 80–120 °C. The dissolution of feldspar can provide considerable amounts of potassium and the higher-temperature conditions corresponding to increasing burial depth. The illitization of the fluvial sandstones is likely to occur in the late burial–diagenetic history and can usually be regarded as an indicator of

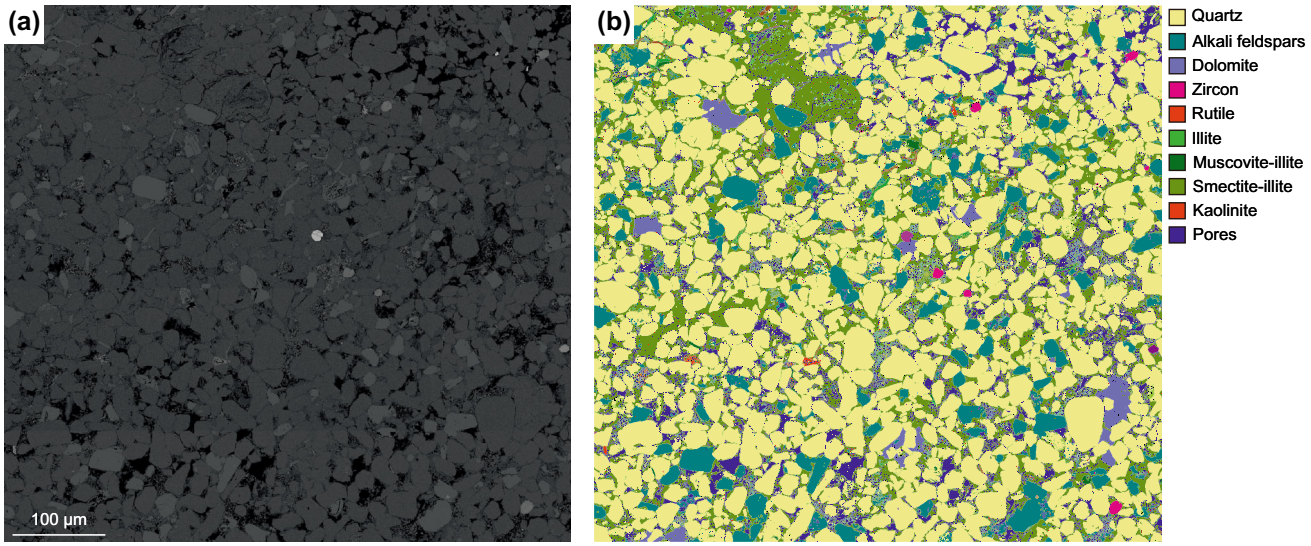

Fig. 11 The BSEM (**a**) and QEMSCAN (**b**) images of a sheet flood deposit; this silty sample contains a higher concentrated illite/smectite which mainly presented as pore-filling aggregates. Sample from Well 30/24-05, 3163.5 m

formation temperatures greater than 100 °C (Bjørlykke et al. 1986; Ehrenberg and Nadeau 1989; Bjorkum et al. 1993).

5.3 Facies and diagenetic controls on reservoir quality

The porosity versus permeability diagrams show that aeolian sandstones generally have better reservoir quality than fluvial sandstones (Fig. 13a). This is partly due to the higher compositional and textural maturity of aeolian deposits, while the fluvial deposits are poorly to moderately sorted, sub-angular to sub-rounded and contain abundant ductile rock fragments. Within each facies, the intergranular porosity of most fluvial channel samples ranges between 10% and 20% with a mean value 15.1%; while other non-channel deposits, such as sheet flood and overbank, have lower porosity that ranged from 0.1% to 15%, and most of them are less than 10% (Fig. 13b). It is also noticeable that the reservoir quality is closely correlated to the lithology variations: channel sandstones which are close to the channel/non-channel interface (< 2 m) contain more rock fragments (Fig. 14a) and less porosity (Fig. 14b), while the channel sandstones which are a considerable distance from the channel/non-channel interface (> 2 m) commonly possess better reservoir quality (Fig. 14). Within aeolian facies, the dune deposits possess an excellent reservoir quality; nearly all the dune sandstone samples have porosity greater than 15% (Fig. 13c). However, the reservoir properties of each sub-facies still show considerable heterogeneity, and this heterogeneity is suggested to have been induced by the subsequent diagenetic processes, which resulted in various diagenetic alterations that controlled reservoir quality (Salem et al. 2005).

Compaction and cementation are two main processes reducing reservoir quality during burial diagenesis (Houseknecht 1987; Ehrenberg 1989; Gluyas and Cade 1997). The relative importance of compaction and cementation on porosity reduction can be quantified using 'measured intergranular porosity-intergranular volume-to-tal cement diagram'. This diagram can be used to evaluate which diagenetic processes have been most influential in porosity reduction (Houseknecht 1987). In this study, the intergranular volume-cement diagram in Fig. 15 shows Buchan Formation data, the total cements include authigenic kaolinite, illite, illite/smectite, dolomite and quartz overgrowth, and the initial porosity is set as 40%.

Compaction exerted a similar average reduction of porosity in both facies sandstones; the mean value 31% and 33% of the initial porosity has been destroyed by compaction in fluvial and aeolian facies, respectively (Fig. 15). However, evidence from petrographic observations reveals that the fluvial sandstones have undergone highly varying degrees of compaction from moderate to intense (1.5%–80.7% of the original porosity has been destroyed by compaction; Fig. 15a). This is supported by the presence of long and concavo-convex grain contacts in the fluvial sandstones, while the aeolian sandstones have only experienced a low to moderate compaction (11.2%–51.5% of the original porosity has been destroyed by compaction; Fig. 15b), as they commonly display point to long grain contacts.

Cementation clearly shows different development in fluvial and aeolian sandstones. Tang et al. (2018) have reported that the primary porosity of aeolian sandstones has

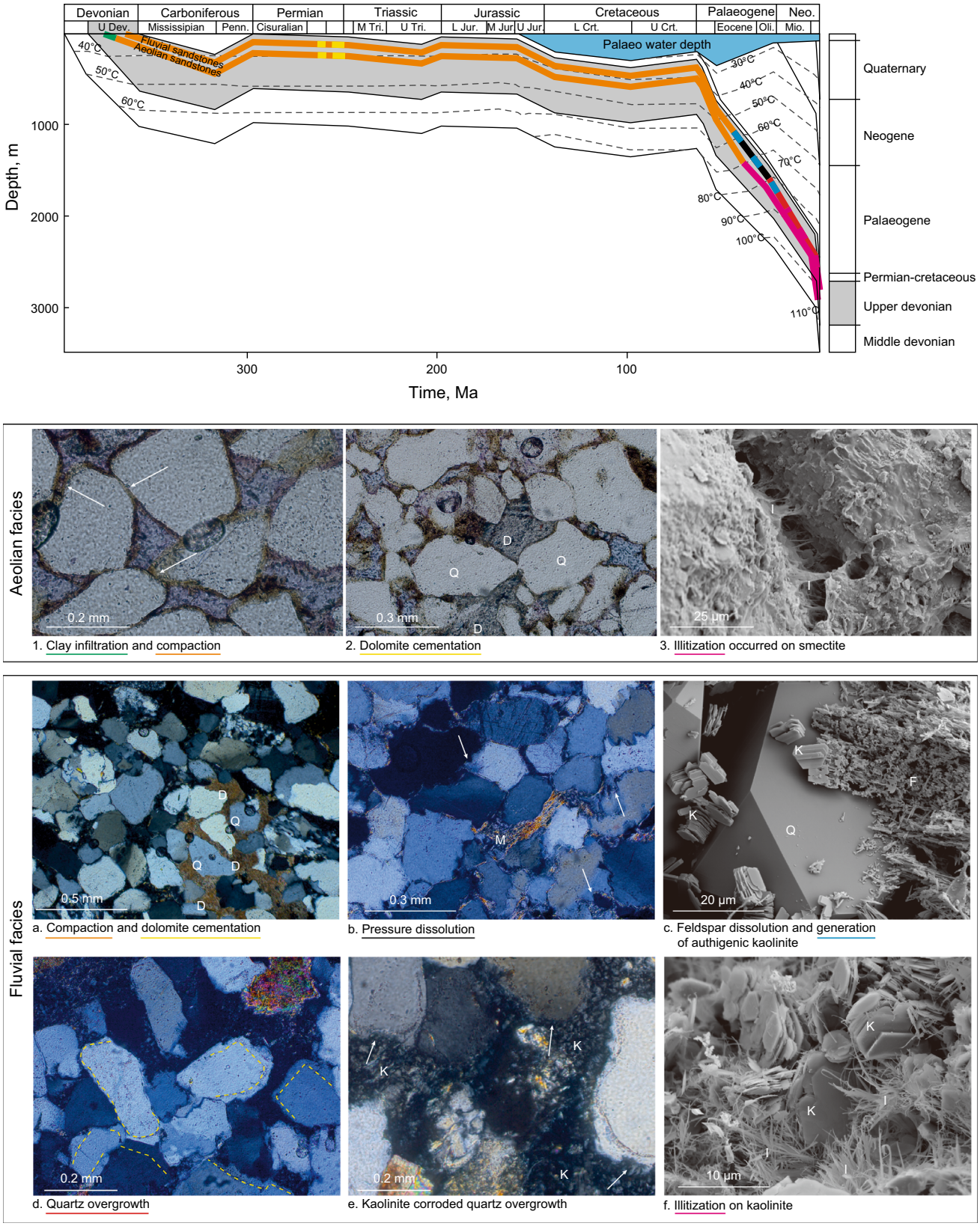

Fig. 12 Paragenesis–burial–thermal history of the Upper Devonian Buchan Formation in the Ardmore Field with corresponding petrographic evidence

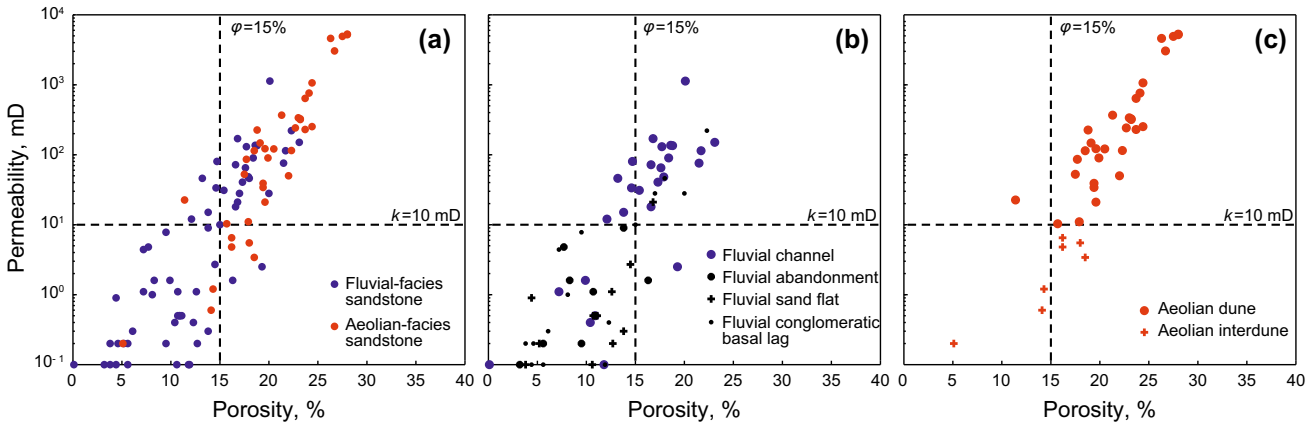

Fig. 13 Porosity–permeability diagrams of: **a** all samples; **b** fluvial-associated samples; **c** aeolian-associated samples. Note porosity = 15% and permeability = 10 mD are set as the lower limit of an effective reservoir

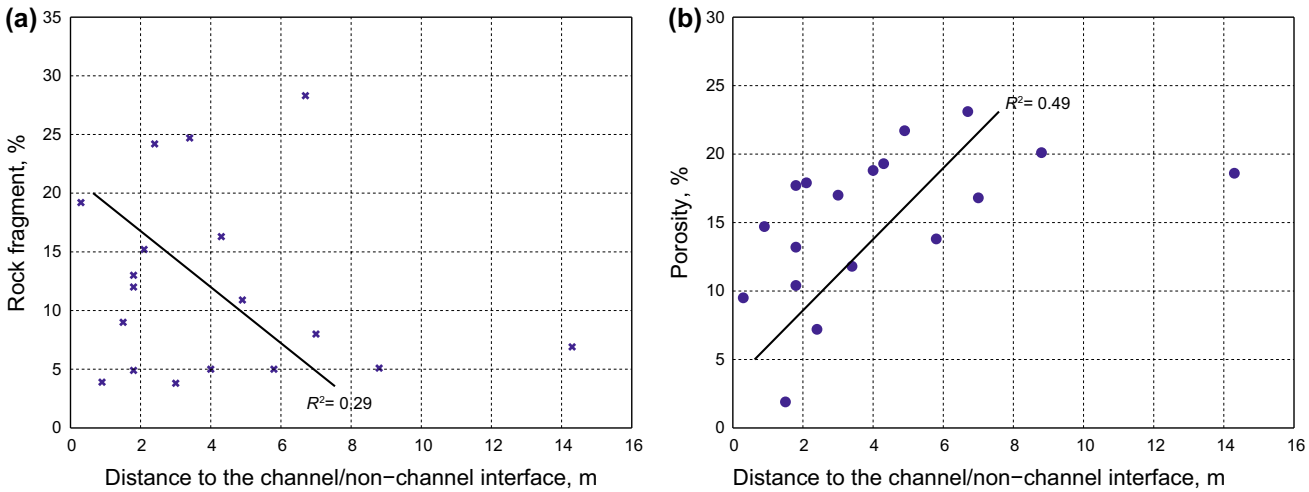

Fig. 14 Diagrams showing relationships: **a** sample point distance to the channel/non-channel interface and amount of rock fragments; **b** sample point distance to the channel/non-channel interface and porosity

been preserved by the early mechanical infiltration of grain-coating illite/smectite, which has inhibited quartz overgrowth development. The calculated results suggest that in the aeolian sandstones, there were only 13% and 26% porosity reduction of dune and interdune facies, respectively, by cementation (Fig. 15b). In comparison, the dolomite cements, authigenic kaolinite and quartz overgrowth in the fluvial sandstones have significantly occupied the pore space. The fluvial channel and non-channel deposits have undergone a loss of 36.4% and 42.9% of the original porosity by cementation, respectively (Fig. 15a).

Compaction and cementation have exerted the major porosity loss in the Buchan Formation. Aeolian sandstones have maintained a better reservoir quality due to the higher compositional and textural maturity, and this would be helpful on keeping primary porosity from mechanical compaction; additionally, with the absence of abundant kaolinite aggregates and the presence of grain-coating illite/smectite which has effectively prevented quartz overgrowth, only sparse dolomite cements have a subordinate effect on reducing porosity. For the fluvial sandstones, lower grain maturity and extensive cementation have significantly reduced porosity. The fluvial intervals with relatively good reservoir quality are mainly composed of the channel sand packages that tended to be isolated from other channel facies.

6 Conclusions

This research into the Upper Devonian Buchan Formation has investigated the source of various cements, reconstructed the sequence of diagenetic events and evaluated their effects on reservoir quality by using diagenetic and geochemical methods. Mechanical compaction exerted similar porosity loss on both aeolian and fluvial sandstones;

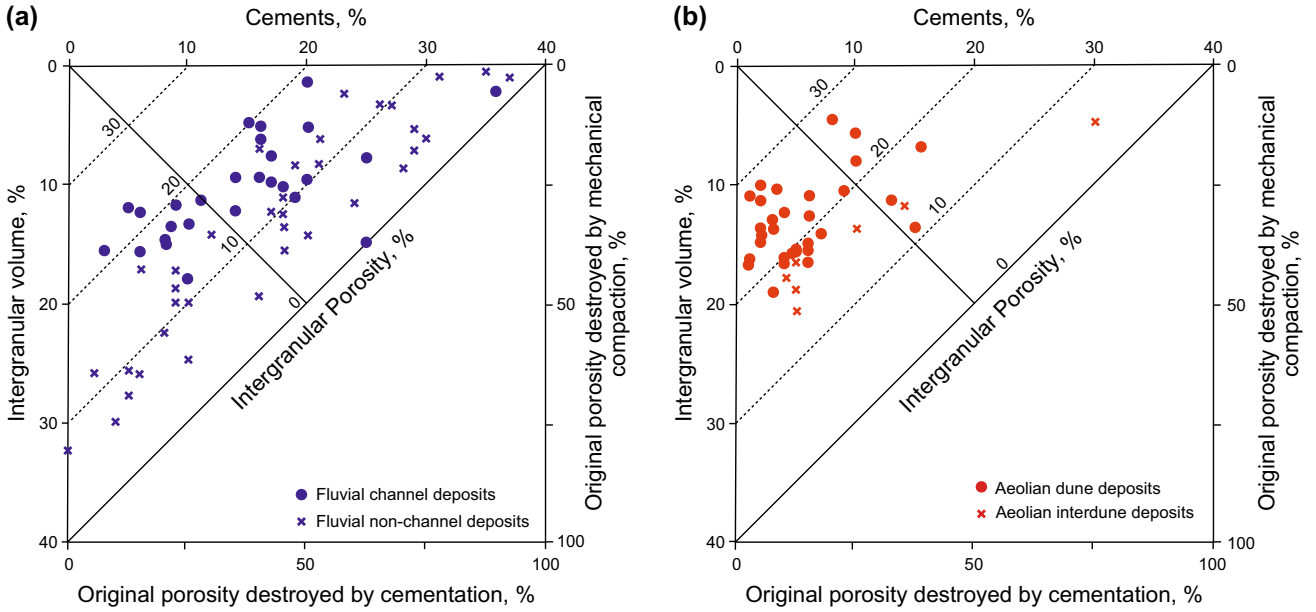

Fig. 15 Intergranular volume versus cement with the importance of compaction/cementation on reducing porosity in different Buchan Formation sedimentary facies. **a** Fluvial-associated samples; **b** aeolian-associated samples

however, cementation of various authigenic minerals shows contrasting differences. Dolomite cementation is prevalent in both sandstone facies; the stable isotope analysis suggested a major marine carbon source and precipitation at a shallow burial depth. The overlying Upper Permian Zechstein carbonate is suggested as the most probable source. The aeolian sandstones contain grain-coating clays that have restricted quartz overgrowth development. Conversely, the fluvial sandstones suffered higher degrees of porosity loss from quartz cementation due to the lack of grain-coating clays. The extensive quartz overgrowths in the fluvial sandstones probably originated from feldspar kaolinitization and pressure dissolution. The homogenization temperature of fluid inclusions (80–120 °C) in the quartz overgrowths and host grains indicates this process occurred at a relatively late stage of burial. Illitization occurred in both aeolian and fluvial sandstones and was suggested to be the last diagenetic event.

This research has important implications for the hydrocarbon exploration of mixed fluvial–aeolian reservoir sandstones where there can be considerable variations in reservoir quality controlled primarily by early grain-coating clays. The results highlight the immense potential for exploration in Devonian mixed fluvial–aeolian reservoirs of mature hydrocarbon provenances such as the Central and Northern North Sea.

Acknowledgements The author thanks EnQuest PLC for supporting this research through access to internal data and financial support of analytical work; British Geological Survey (BGS) is thanked for its assistance in facilitating the examination of Devonian cores. We are all grateful for the expertise and general assistance offered by Mr. Ian Chaplin (Department of Earth Sciences, Durham University) and the assistance on preparing isotopic samples from Dr. Geoff Nowell (Department of Earth Sciences, Durham University). Thanks too are given to Professor Adrian Boyce of SUERC for undertaking the isotope analysis and Miss Jenny Omma of Rocktype for undertaking the QEMSCAN analysis.

References

Bifani R, Smith C. The Argyll field after a decade of production. SPE J. 1985. https://doi.org/10.2118/13987-MS.

Bjorkum PA, Walderhaug O, Aase NE. A model for the effect of illitization on porosity and quartz cementation of sandstones. J Sediment Res. 1993;63(6):1089–91. https://doi.org/10.2110/jsr.63.1089.

Bjørlykke K. Diagenetic reactions in sandstones. In: Parker A, Sellwood BW, editors. Sediment diagenesis. NATO ASI Series (Series C: Mathematical and Physical Sciences). vol 115. Dordrecht: Springer; 1983. p. 169–213.

Bjorlykke K, Jahren J. Open or closed geochemical systems during diagenesis in sedimentary basins: constraints on mass transfer during diagenesis and the prediction of porosity in sandstone and carbonate reservoirs. AAPG Bull. 2012;96(12):2193–214. https://doi.org/10.1306/04301211139.

Bjørlykke K, Aagaard P, Dypvik H, Hastings D, Harper A. Diagenesis and reservoir properties of Jurassic sandstones from the Haltenbanken area, offshore mid-Norway. In: Graham &

Trotman, editors. Habitat of hydrocarbons on the Norwegian continental shelf. London; 1986. p. 275–86.
Bjørlykke K, Mo A, Palm E. Modelling of thermal convection in sedimentary basins and its relevance to diagenetic reactions. Mar Pet Geol. 1988;5(4):338–51. https://doi.org/10.1016/0264-8172(88)90027-X.
Bradshaw M, et al. Atlas of palaeogeography and lithofacies. London: The Geological Society; 1992.
Burley S. Patterns of diagenesis in the Sherwood Sandstone Group (Triassic), United Kingdom. Clay Miner. 1984;19(3):403–40. https://doi.org/10.1180/claymin.1984.019.3.11.
Coplen TB, Kendall C, Hopple J. Comparison of stable isotope reference samples. Nature. 1983;302(5905):236–8. https://doi.org/10.1038/302236a0.
Downie R. Devonian. In: Glennie KW, editor. Petroleum geology of the North Sea: basic concepts and recent advances. 4th ed. Oxford: Blackwell Science; 2009. p. 85–103.
Edwards C. The Buchan Field, Blocks 20/5a and 21/1a, UK North Sea. Geol Soc Lond Mem. 1991;14(1):253–9. https://doi.org/10.1144/GSL.MEM.1991.014.01.31.
Ehrenberg S. Assessing the relative importance of compaction processes and cementation to reduction of porosity in sandstones: discussion; compaction and porosity evolution of Pliocene sandstones, Ventura Basin, California: discussion. AAPG Bull. 1989;73(10):1274–6.
Ehrenberg S, Nadeau P. Formation of diagenetic illite in sandstones of the Garn Formation, Haltenbanken area, mid-Norwegian continental shelf. Clay Miner. 1989;24(2):233–53. https://doi.org/10.1180/claymin.1989.024.2.09.
Evans G, Schmidt V, Bush P, Nelson H. Stratigraphy and geologic history of the sabkha, Abu Dhabi, Persian Gulf. Sedimentology. 1969;12(1-2):145–59. https://doi.org/10.1111/j.1365-3091.1969.tb00167.x.
Folk RL. Petrology of sedimentary rocks. Austin: Hemphill Publishing Company; 1980. p. 2–3.
Gambaro M, Currie M. The Balmoral, Glamis and Stirling fields, block 16/21, UK Central North Sea. Geol Soc Lond Mem. 2003;20(1):395–413. https://doi.org/10.1144/GSL.MEM.2003.020.01.33.
Glennie K. Petroleum Geology of the North Sea: basic concepts and recent advances. London: Wiley; 2009. p. 89–103.
Glennie K, Provan D. Lower Permian Rotliegend reservoir of the southern North Sea gas province. Geol Soc Lond Spec Publ. 1990;50(1):399–416. https://doi.org/10.1144/GSL.SP.1990.050.01.25.
Gluyas J. Zechstein carbonates as a petroleum reservoir, Argyll/Ardmore Field, UK Continental Shelf. Proc Open Univ Geol Soc. 2016;2:39–45.
Gluyas J, Cade CA. Prediction of porosity in compacted sands. In: AAPG memoir: reservoir quality prediction in sandstones and carbonates, vol. 69; 1997. p. 19–27.
Gluyas JG, Mair B, Schofield P, Arkley P, McRae D. Ardmore field: rebirth of the first offshore oil field, UKCS. In: Geological Society, London, petroleum geology conference series, vol. 6; 2005, p. 367–88. https://doi.org/10.1144/0060367.
Hayward R, Martin C, Harrison D, Van Dort G, Guthrie S, Padget N. The Flora field, blocks 31/26a, 31/26c, UK north sea. Geol Soc Lond Mem. 2003;20(1):549–55. https://doi.org/10.1144/GSL.MEM.2003.021.01.44.
Heward AP, Schofield P, Gluyas JG. The Rotliegend reservoir in Block 30/24, UK Central North Sea: including the Argyll (renamed Ardmore) and Innes Fields. Pet Geosci. 2003;9(4):295–307. https://doi.org/10.1144/1354-079303-578.
Hoffman J, Hower J. Clay mineral assemblages as low grade metamorphic geothermometers: application to the thrust faulted disturbed belt of Montana, USA. In: SEPM Special Publication No 26; 1979. p. 55–79.
Houseknecht DW. Assessing the relative importance of compaction processes and cementation to reduction of porosity in sandstones. AAPG Bull. 1987;71(6):633–42.
Howell J, Mountney N. Climatic cyclicity and accommodation space in arid to semi-arid depositional systems: an example from the Rotliegend Group of the UK southern North Sea. Geol Soc Lond Spec Publ. 1997;123(1):63–86. https://doi.org/10.1144/GSL.SP.1997.123.01.05.
Huang W-L, Longo JM, Pevear DR. An experimentally derived kinetic model for smectite-to-illite conversion and its use as a geothermometer. Clays Clay Miner. 1993;41:162. https://doi.org/10.1346/CCMN.1993.0410205.
Keith M, Weber JN. Carbon and oxygen isotopic composition of selected limestones and fossils. Geochim Cosmochim Acta. 1964;28(10-11):1787–816. https://doi.org/10.1016/0016-7037(64)90022-5.
Keller W, Reynolds R, Inoue A. Morphology of clay minerals in the smectite-to-illite conversion series by scanning electron microscopy. Clays Clay Miner. 1986;34(2):187–97. https://doi.org/10.1346/CCMN.1986.0340209.
Kinsman DJ. Modes of formation, sedimentary associations, and diagnostic features of shallow-water and supratidal evaporites. AAPG Bull. 1969;53(4):830–40.
Knight I, Allen L, Coipel J, Jacobs L, Scanlan M. The Embla field. In: Geological Society, London, petroleum geology conference series, vol. 4; 1993. p. 1433–44. https://doi.org/10.1144/0041433.
Leveille GP, Primmer TJ, Dudley G, Ellis D, Allinson GJ. Diagenetic controls on reservoir quality in Permian Rotliegendes sandstones, Jupiter Fields area, southern North Sea. Geol Soc Lond Spec Publ. 1997;123(1):105–22. https://doi.org/10.1144/GSL.SP.1997.123.01.06.
Marshall JEA, Hewett AJ. Devonian. In: Graham C, Armour A, Bathurst P, Evans D, Petroleumsforening N, editors. The Millennium Atlas: petroleum geology of the central and northern North Sea. London: Geol Soc Lond; 2003. p. 65–81.
Matthews A, Katz A. Oxygen isotope fractionation during the dolomitization of calcium carbonate. Geochim Cosmochim Acta. 1977;41(10):1431–8. https://doi.org/10.1016/0016-7037(77)90249-6.
McKinley J, Worden R, Ruffell A. Smectite in sandstones: a review of the controls on occurrence and behaviour during diagenesis. In: Worden RH, Morad S, editors. Clay mineral cements in sandstones: international association of sedim-entologists special publication, vol. 34; 2003. p. 109–28. https://doi.org/10.1002/9781444304336.
Nagtegal P. Relationship of facies and reservoir quality in Rotliegendes desert sandstones, southern North Sea region. J Pet Geol. 1979;2(2):145–58. https://doi.org/10.1111/j.1747-5457.1979.tb00699.x.
Purvis K. Lower Permian Rotliegend sandstones, southern North Sea: a case study of sandstone diagenesis in evaporite-associated sequences. Sed Geol. 1992;77(3-4):155–71. https://doi.org/10.1016/0037-0738(92)90123-9.
Pye K, Krinsley D. Diagenetic carbonate and evaporite minerals in Rotliegend aeolian sandstones of the southern North Sea: their nature and relationship to secondary porosity development. Clay Miner. 1986;21(4):443–57. https://doi.org/10.1180/claymin.1986.021.4.03.
Robinson A, Gluyas J. Duration of quartz cementation in sandstones, North Sea and Haltenbanken Basins. Mar Pet Geol. 1992;9(3):324–7. https://doi.org/10.1016/0264-8172(92)90081-O.

Robson D. The Argyll, Duncan and Innes Fields, Block 30/24 and 30/25a, UK North Sea. Geol Soc Lond Mem. 1991;14(1):219–26. https://doi.org/10.1144/GSL.MEM.1991.014.01.27.

Salem AM, Ketzer J, Morad S, Rizk RR, Al-Aasm I. Diagenesis and reservoir-quality evolution of incised-valley sandstones: evidence from the Abu Madi gas reservoirs (Upper Miocene), The Nile Delta Basin, Egypt. J Sediment Res. 2005;75(4):572–84. https://doi.org/10.2110/jsr.2005.047.

Selley R. Porosity gradients in North Sea oil-bearing sandstones. J Geol Soc. 1978;135(1):119–32. https://doi.org/10.1144/gsjgs.135.1.0119.

Shelton JW. Authigenic kaolinite in sandstone. J Sediment Res. 1964;34(1):102–11.

Sweet M. Interaction between aeolian, fluvial and playa environments in the Permian Upper Rotliegend Group, UK southern North Sea. Sedimentology. 1999;46(1):171–88. https://doi.org/10.1046/j.1365-3091.1999.00211.x.

Talbot M. A review of the palaeohydrological interpretation of carbon and oxygen isotopic ratios in primary lacustrine carbonates. Chem Geol Isot Geosci Sect. 1990;80(4):261–79. https://doi.org/10.1016/0168-9622(90)90009-2.

Tang L, Jones SJ, Gluyas JG. Porosity preservation due to grain coating illite/smectite: evidence from Buchan Formation (Upper Devonian) of the Ardmore Field, UK North Sea. In: Proceedings of the geologists' association; 2018 **(accepted, in press).**

Tang L, Jones SJ, Gluyas JG. Facies Architecture of the Fluvial-Aeolian Buchan formation (Upper Devonian) and its implications on field exploration: a case study from Ardmore Field, Central North Sea, UK. International Journal of Geosciences. 2017;8(07):902. https://doi.org/10.4236/ijg.2017.87052.

Tournier F, Pagel M, Portier E, Wazir I, Fiet N. Relationship between deep diagenetic quartz cementation and sedimentary facies in a Late Ordovician glacial environment (Sbaa Basin, Algeria). J Sediment Res. 2010;80(12):1068–84. https://doi.org/10.2110/jsr.2010.094.

Trewin NH, Bramwell MG. The Auk Field, Block 30/16, UK North Sea. Geol Soc Lond Mem. 1991;14(1):227–36. https://doi.org/10.1144/GSL.MEM.2003.020.01.39.

Vitali F, Blanc G, Larqué P, Duplay J, Morvan G. Thermal diagenesis of clay minerals within volcanogenic material from the Tonga convergent margin. Mar Geol. 1999;157(1):105–25. https://doi.org/10.1016/S0025-3227(98)00134-0.

Walderhaug O. Modeling quartz cementation and porosity in Middle Jurassic Brent Group sandstones of the Kvitebjørn field, northern North Sea. AAPG Bull. 2000;84(9):1325–39. https://doi.org/10.1306/A9673E96-1738-11D7-8645000102C1865D.

Wilson MD, Pittman ED. Authigenic clays in sandstones: recognition and influence on reservoir properties and paleoenvironmental analysis. J Sediment Res. 1977. https://doi.org/10.1306/212F70E5-2B24-11D7-8648000102C1865D.

Wilson M, Wilson L, Patey I. The influence of individual clay minerals on formation damage of reservoir sandstones: a critical review with some new insights. Clay Miner. 2014;49(2):147–64. https://doi.org/10.1180/claymin.2014.049.2.02.

Yuan G, et al. Diagenesis and reservoir quality evolution of the Eocene sandstones in the northern Dongying Sag, Bohai Bay Basin, East China. Mar Pet Geol. 2015;62:77–89. https://doi.org/10.1016/j.marpetgeo.2015.01.006.

Ziegler PA. Geological atlas of western and central Europe. London: Geol Soc Lond; 1990. p. 13–6.